J Membrane Biol (2010) 238:21–31
DOI 10.1007/s00232-010-9315-9

Effects of Mutations Within Surface-Exposed Loops in the Pore-Forming Domain of the Cry9Ca Insecticidal Toxin of *Bacillus thuringiensis*

Jean-Frédéric Brunet · Vincent Vachon · Mireille Marsolais · Greta Arnaut · Jeroen Van Rie · Lucie Marceau · Geneviève Larouche · Charles Vincent · Jean-Louis Schwartz · Raynald Laprade

Received: 15 April 2010 / Accepted: 27 October 2010 / Published online: 17 November 2010

Abstract The pore-forming domain of *Bacillus thuringiensis* insecticidal Cry toxins is formed of seven amphipathic α-helices. Because pore formation is thought to involve conformational changes within this domain, the possible role of its interhelical loops in this crucial step was investigated with Cry9Ca double mutants, which all share the previously characterized R164A mutation, using a combination of homology modeling, bioassays and electrophysiological measurements. The mutations either introduced, neutralized or reversed an electrical charge carried by a single residue of one of the domain I loops. The ability of the 28 Cry9Ca double mutants to depolarize the apical membrane of freshly isolated *Manduca sexta* larval midguts was tested in the presence of either midgut juice or a cocktail of protease inhibitors because these conditions had been shown earlier to greatly enhance pore formation by Cry9Ca and its R164A single-site mutant. Most mutants retained toxicity toward neonate larvae and a pore-forming ability in the electrophysiological assay, which were comparable to those of their parental toxin. In contrast, mutants F130D, L186D and V189D were very poorly toxic and practically inactive in vitro. On the other hand, mutant E129A depolarized the midgut membrane efficiently despite a considerably reduced toxicity, and mutant Q192E displayed a reduced depolarizing ability while conserving a near wild-type toxicity. These results suggest that the conditions found in the insect midgut, including high ionic strength, contribute to minimizing the influence of surface charges on the ability of Cry9Ca and probably other *B. thuringiensis* toxins to form pores within their target membrane.

Keywords Insecticidal toxin · Homology modeling · Pore formation · Membrane potential · Electrostatic interaction · *Bacillus thuringiensis* · *Manduca sexta*

J.-F. Brunet (✉) · V. Vachon · M. Marsolais · L. Marceau · J.-L. Schwartz · R. Laprade
Groupe d'étude des protéines membranaires, Université de Montréal, P.O. Box 6128, Centre Ville Station, Montreal, QC H3C 3J7, Canada
e-mail: jean-frederic.brunet@umontreal.ca

R. Laprade
e-mail: raynald.laprade@umontreal.ca

G. Arnaut · J. Van Rie
Bayer BioScience NV, Ghent, Belgium

G. Larouche · C. Vincent
Horticultural Research and Development Center, Agriculture and Agri-Food Canada, Saint-Jean-sur-Richelieu, QC J3B 3E6, Canada

Introduction

Bacillus thuringiensis produces a variety of pore-forming toxins that accumulate in the form of crystalline parasporal inclusion bodies during sporulation. The most extensively studied of these are insecticidal (Schnepf et al. 1998; de Maagd et al. 2003; Bravo et al. 2007), but others, specifically toxic to other organisms, including in particular nematodes (Wei et al. 2003; Griffitts and Aroian 2005) and cancer cells (Ohba et al. 2009), have also attracted considerable attention in recent years.

Among the insecticidal members of this protein family, eight have so far had their crystal structure solved: Cry1Aa (Grochulski et al. 1995), Cry1Ac (Li et al. 2001), Cry2Aa (Morse et al. 2001), Cry3Aa (Li et al. 1991), Cry3Bb (Galitsky et al. 2001), Cry4Aa (Boonserm et al. 2006), Cry4Ba (Boonserm et al. 2005) and Cry8Ea (Guo et al. 2009). Despite a relatively low degree of homology between their amino acid sequences, these toxins all display a remarkably

similar three-domain structure. Whereas domain I, a bundle of seven amphipathic α-helices, is responsible for membrane insertion and pore formation (Li et al. 1991; Grochulski et al. 1995), domain II, a region composed of three antiparallel β-sheets with Greek key topology arranged in a β-prism, and domain III, two antiparallel β-sheets forming a β-sandwich with a jelly-roll topology, are involved in receptor binding, prior to pore formation, and toxin specificity (Gómez et al. 2007; Pigott and Ellar 2007). Although the mechanism of pore formation is still the subject of intensive research, it probably involves conformational changes in the toxin molecule. These imply, in particular, rotations about the polypeptide backbone in domain I interhelical loops. Until recently, however, these loops have received only limited attention (Girard et al. 2009; Lebel et al. 2009).

Cry9Ca, a toxin which is active against a variety of lepidopteran insects, is also known to be particularly sensitive to proteolysis (Lambert et al. 1996). Although its main proteolysis site has been removed by site-directed mutagenesis in its R164A mutant (Lambert et al. 1996), recent experiments have suggested that other proteolysis sites may affect its activity, at least during in vitro experiments performed in the presence of its target membrane, the brush border membrane located on the apical side of insect larval midgut epithelial columnar cells (Brunet et al. 2010b). Osmotic swelling experiments with brush border membrane vesicles have also indicated that the pore-forming ability of Cry9Ca depends strongly on the pH of the solutions in which they are performed (Brunet et al. 2010a). This observation suggests that electrostatic interactions between surface-exposed residues on the toxin and its receptor protein could play a major role in pore formation.

In the present study, the three-dimensional structure of Cry9Ca was modeled by homology and its mode of action was further studied by examining the toxicity and pore-forming properties of a variety of double mutants, all derived from the single-site mutant R164A, in which an electrical charge was either neutralized, introduced or reversed in selected residues located within or very near surface-exposed interhelical loops of domain I. The in vitro conditions used for these experiments were those that had previously been found to optimize the activity of wild-type Cry9Ca and its R164A mutant at physiological pH. With few exceptions, the toxicity and pore-forming ability of most of the mutants were comparable to those of their parental toxin.

Materials and Methods

Homology Model

The three-dimensional structure of Cry9Ca was modeled by homology with SWISS-MODEL software (http://swissmodel.expasy.org) (Peitsch 1995, 1996; Guex and Peitsch 1997), using the known structures of Cry1Aa (PDB file 1CIY), Cry2Aa (PDB file 1I5PA) and Cry3Aa (PDB file 1DLC) as templates. The resulting model was analyzed with Swiss PdbViewer (version 3.7b2; Glaxo Wellcome Experimental Research, Plan-les-Ouates, Switzerland).

Site-Directed Mutagenesis

The R164A mutant of Cry9Ca (Lambert et al. 1996) was the parental toxin from which all double mutants reported in the present study were derived. Second mutations were introduced by individually altering selected domain I loop residues by site-directed mutagenesis, using a polymerase chain reaction technique described by Ho et al. (1989). The double mutants are referred to by simply stating the second substitution which makes them unique. All mutants analyzed in the present study and the positions of their mutated residues within the toxin structure are listed in Table 1.

Toxin Activation and Purification

All Cry9Ca mutants were prepared from *Escherichia coli* W6K strains, producing the appropriate single recombinant toxins as described previously (Lambert et al. 1996). Protoxins were trypsin-activated in vitro, and the resulting toxins were purified by fast protein liquid chromatography using a mono-Q ion exchange column (Pharmacia Biotech, Montreal, QC, Canada) as described elsewhere (Masson et al. 1990, 1994).

Bioassays

Fertilized *Manduca sexta* eggs were purchased from the insectary of the North Carolina State University Department of Entomology (Raleigh, NC). Larvae were reared on an artificial diet obtained from the same source. Toxicity was evaluated with neonate larvae that were fed an artificial diet contaminated with toxin as described earlier (Coux et al. 2001). Activated toxins were applied as 100-µl samples that were layered onto 1.8-cm^2 wells and allowed to absorb into the medium. Each mutant was tested on 10 different occasions with 25 larvae for each toxin concentration. Mortality and, for surviving insects, weight gain were recorded after 7 days. Data were adjusted for the mortality of control larvae reared in the absence of toxin. Tests were first carried out with 10 µg of toxin/ml, corresponding to 555 ng of toxin/cm^2, a value slightly above our experimental LC_{90} for Cry9Ca R164A (460 ng/cm^2) (Brunet et al. 2010a). When appreciable toxicity was

Table 1 Toxicity of Cry9Ca mutants to *M. sexta* neonate larvae

Mutation	Mutation site	% Mortality[a] at		
		5 μg/ml	10 μg/ml	50 μg/ml
R164A[b] (parental toxin)	α3–α4 loop	58 (28–79)[c]	95 (77–99)[c]	–[d]
E121A	α2b-helix	97 ± 2	100 ± 0	–
E121K	α2b-helix	95 ± 2	100 ± 0	–
N124D	α2–α3 loop	90 ± 2	99.4 ± 0.6	–
N124R	α2–α3 loop	92 ± 3	99 ± 1	–
Q125E	α2–α3 loop	79 ± 8	99.5 ± 0.5	–
Q126E	α2–α3 loop	90 ± 4	100 ± 0	–
T128D	α2–α3 loop	66 ± 6	92 ± 7	–
E129A	α3-helix	8 ± 2	46 ± 9	–
E129K	α3-helix	49 ± 5	88 ± 5	–
F130D	α3-helix	–	0 ± 3	18 ± 4
L186D	α4–α5 loop	–	2 ± 2	3 ± 2
F187D	α4–α5 loop	96 ± 2	100 ± 0	–
V189D	α4–α5 loop	–	5 ± 3	30 ± 7
N190C	α4–α5 loop	52 ± 10	97 ± 1	–
N190R	α4–α5 loop	97 ± 1	100 ± 0	–
Q192E	α4–α5 loop	36 ± 4	85 ± 3	–
Q193E	α5-helix	66 ± 8	90 ± 3	–
T224R	α5–α6 loop	70 ± 5	98.4 ± 0.8	–
D255K	α6-helix	77 ± 5	97 ± 2	–
R256D	α6-helix	51 ± 6	93 ± 2	–
R258D	α6–α7 loop	64 ± 7	98 ± 1	–
T260D	α6–α7 loop	54 ± 7	99.0 ± 0.7	–
T260R	α6–α7 loop	62 ± 7	97 ± 2	–
N261D	α6–α7 loop	63 ± 10	100 ± 0	–
N261R	α6–α7 loop	46 ± 10	97 ± 1	–
E263K	α7-helix	86 ± 4	99.2 ± 0.5	–
P295R	α7–β1 loop	62 ± 8	96 ± 3	–
T296R	β1-strand	81 ± 5	97 ± 1	–

[a] Except for R164A, values are means ± standard error of the mean (SEM) of 10 independent experiments

[b] This substitution is present in all mutants in addition to the indicated second mutation

[c] Data for the single-site mutant R164A were evaluated from the dose–response curves used to estimate the LC_{50} and LC_{90} values reported by Brunet et al. (2010a). 95% Confidence intervals are shown in parentheses

[d] –, not tested

observed at this first concentration, a second series of tests was carried out at 5 μg of toxin/ml (278 ng/cm^2), a value near our Cry9Ca R164A LC_{50} value (250 ng/cm^2) (Brunet et al. 2010a). Alternatively, when the mutants displayed poor toxicity at the first concentration, they were tested at 50 μg/ml (2.78 μg/cm^2).

Midgut Isolation and Midgut Juice Preparation

For membrane potential measurements, whole midguts were isolated from third-instar larvae as described by Peyronnet et al. (1997) and bathed in the 122 K solution consisting of 122 mM KCl, 5 mM $CaCl_2$ and 5 mM 3-(cyclohexylamino)-1-propanesulfonic acid (CAPS)–KOH (pH 10.5). Midgut juice was collected from whole midguts isolated from fifth-instar larvae as described by Fortier et al. (2007) and stored at –80°C in small aliquots.

Membrane Potential Measurements

Short segments of freshly isolated *M. sexta* midguts were aspirated into a glass pipette from one end until the other end curled around the pipette tip, thus exposing the apical surface of the epithelial cells (Peyronnet et al. 1997). The pipette was lowered near the bottom of a perfusion chamber containing the 122 K solution, and midgut cells were impaled with a glass microelectrode filled with 1 M KCl (Peyronnet et al. 1997). Electrode resistance was between 50 and 250 MΩ. Impalements were considered successful when they caused a sharp and sustained change in the measured potential (negative inside). The bath was perfused continuously with the 122 K solution until the membrane potential was stable for 5 min. Perfusion was then stopped, and the perfusion solution was replaced by 1.2 ml of the 122 K solution containing 5 μg/ml of the

appropriate toxin with either 10% (v/v) midgut juice or 1% (v/v) of a protease inhibitor cocktail (described below). After 5 min, the preparation was rinsed with the 122 K solution for an additional 10 min. Experiments were carried out at room temperature. When midgut juice was added, it was first diluted sufficiently in a solution composed of 5 mM $CaCl_2$ and 5 mM CAPS-KOH (pH 10.5) to reach a potassium concentration of 122 mM (Fortier et al. 2007). The final volume was then adjusted with the 122 K solution. The protease inhibitor cocktail contained 50 mM 4-(aminoethyl)benzenesulfonyl fluoride (AEBSF), 1 mg/ml antipain, 0.015 mM aprotinin, 0.1 mM trans-epoxysuccinyl-L-leucylamido-(4-guanidino)butane (E64) and 0.1 mM leupeptin dissolved in water and used at a final 100-fold dilution. All of these compounds were obtained from Sigma-Aldrich (Oakville, ON, Canada).

Results

Overall Structure

The online SWISS-MODEL software (Peitsch 1995, 1996; Guex and Peitsch 1997) returned a model of the three-dimensional structure of Cry9Ca a few hours after its sequence was submitted. The model covers the portion of the protein extending from residue 65 (Ser) to residue 658 (Asn). The familiar three-domain structure of Cry toxins is readily recognizable (Fig. 1a), with domain I and its seven α-helices ranging from residue 65 to residue 292 (except 84–87), domain II in the form of a β-prism made up of three β-sheets ranging from residue 303 to residue 504 and domain III, a β-sandwich, including residues 84–87, 293–302 and 505–658.

The presence of a short segment between domains I and II in the linear sequence (residues 293–302, which include β1a) but belonging to domain III has been described for the corresponding portion of Cry1Aa (Grochulski et al. 1995). However, residues 84–87, belonging to the α1–α2a loop, are also predicted to form a short β-strand that is strongly connected to β1a and, thus, to form an integral part of the domain III β-sandwich (Fig. 1b). To our knowledge, this is the first time a segment of the α1–α2a loop has been suggested to constitute part of domain III since this was not reported for the above-mentioned toxins for which the crystal structure has been elucidated or for those toxins for which a structure has been proposed on the basis of homology modeling (Alcantara et al. 2001; Gutierrez et al. 2001; Angsuthanasombat et al. 2004; Fernández et al. 2005; Lin et al. 2008; Xia et al. 2008; Yamaguchi et al. 2008; Likitvivatanavong et al. 2009; Zhao et al. 2009).

Although the predicted structure of Cry9Ca appears otherwise very similar to those of the toxins used as templates for the modeling, a few other noticeable differences were identified. In domain I, the most obvious differences between Cry9Ca and Cry1Aa, Cry2Aa and Cry3Aa are its longer α2a–α2b loop and its α3–α4 loop that protrudes away from the domain core, making it more accessible than in any of the other three toxins (Fig. 2a). In domain II, the three usual β-sheets are found, but Cry9Ca is predicted to form an unstructured coil in place of the β9-strand, which is present in the other three toxins (Fig. 2b). In domain III, one major difference is found within the β19–β20 loop (Fig. 2c). Not only is it longer than in the other three toxins, but it is predicted to form a short α-helix, which runs close to α6 of domain I.

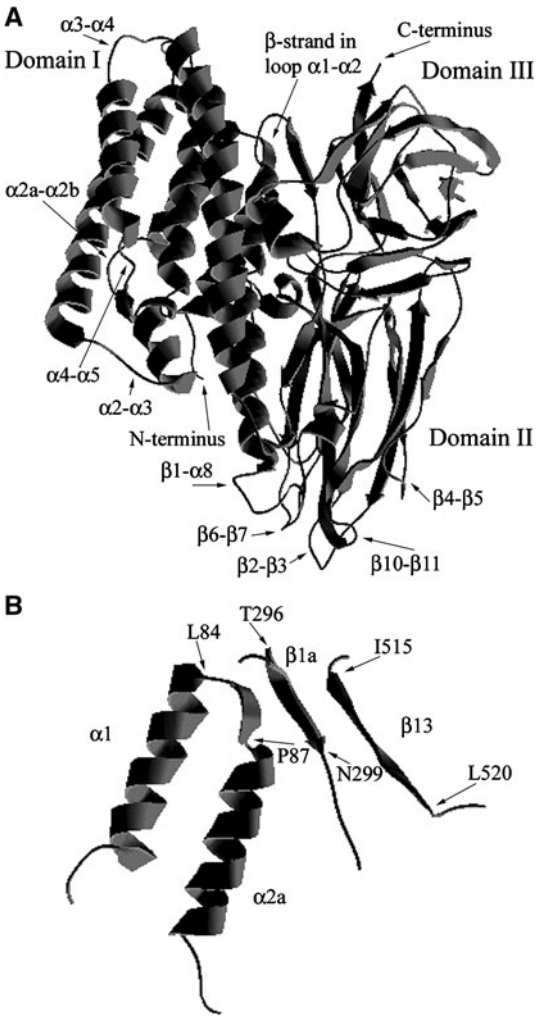

Fig. 1 Homology model of Cry9Ca. **a** This tentative three-dimensional structure of Cry9Ca was established by homology modeling using the SWISS-MODEL program on the basis of the published structures of Cry1Aa, Cry2Aa and Cry3Aa. **b** The model predicts the existence in Cry9Ca of a novel structural pattern in which a small β-strand, located within the α1–α2 loop, contributes to the β-sheet structure of domain III formed by the β13, β14, β15, β17, β20, β21 and β23 strands in addition to the β1a-strand, which is located between domains I and II in the linear sequence of the toxin and interacts directly with the β13-strand

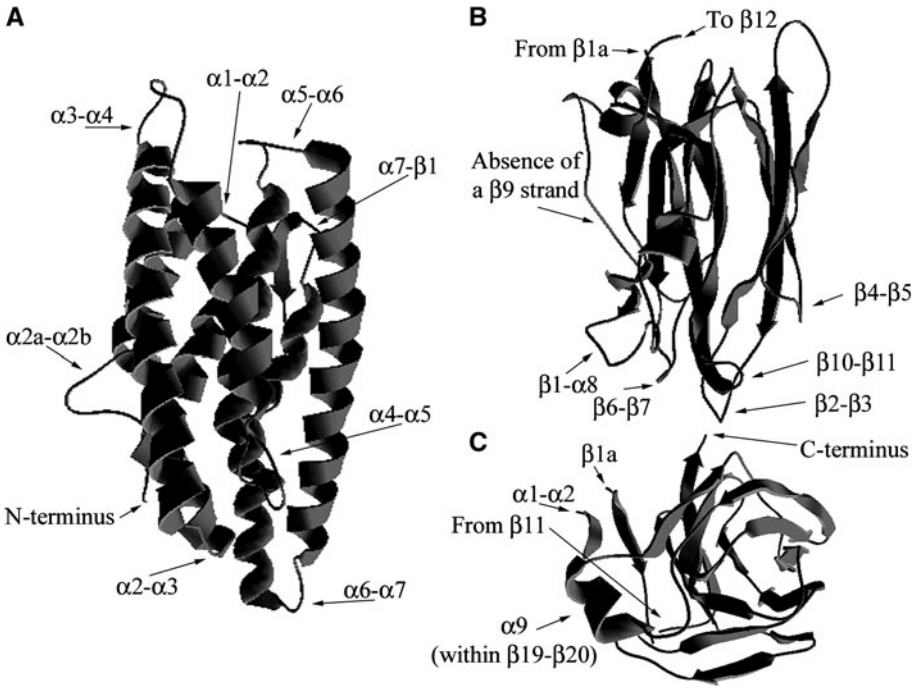

Fig. 2 Main features of the Cry9Ca model. **a** Domain I displayed after a 90° counterclockwise rotation with respect to the orientation shown in Fig. 1a to emphasize its unusually long α2a–α2b loop and its α3–α4 loop, which is predicted by the model to protrude away from the core of the protein. **b** Domain II shown in the same orientation as in Fig. 1a. The most remarkable prediction of the model, in this region of the toxin, is the absence of the *β*9-strand, which is found in the structure of the three toxins used as templates. **c** Structure of domain III, also reproduced in the same orientation as in Fig. 1a, in which a novel α-helix (α9) is predicted to lie within the *β*19–*β*20 loop of Cry9Ca

Toxicity

The toxicity of most double mutants (Table 1) was comparable to that estimated for the parental toxin (R164A) on the basis of dose–response curves that were used to evaluate, by probit analysis, previously reported values of LC_{50} and LC_{90} (Brunet et al. 2010a). When tested at 10 μg toxin/ml, all mutants except E129A, F130D, L186D and V189D killed at least 80% of the larvae, a level which falls within the 95% confidence interval estimated for the parental toxin. When tested at 5 μg toxin/ml, mutants T128D, E129K, N190C, Q192E, Q193E, T224R, D255K, R256D, R258D, T260D, T260R, N261D, N261R and P295R killed 36–79% of the larvae, within the 95% confidence interval estimated, at this toxin concentration, for the parental toxin. Somewhat higher percent mortality values were recorded for the other mutants, E121A, E121K, N124D, N124R, Q126E, F187D, N190R, E263K and T296R. Among the four mutants with reduced activity, three were practically inactive and displayed 30% mortality (V189D) or less (F130D and L186D) when tested at 50 μg toxin/ml (Table 1), a concentration which corresponds to more than 10 times the LC_{50} estimated for the parental toxin (Brunet et al. 2010a).

Except for mutant L186D, those mutants with a reduced ability to kill the larvae nevertheless retained some toxicity, as evidenced from weight-gain measurements. While control larvae, reared in the absence of toxin, gained 126 ± 10 mg during the time course of the experiments, larvae which survived treatment with 10 μg/ml of mutants E129A, F130D and V189D gained only 8 ± 1, 81 ± 11 and 71 ± 8 mg, respectively, during the same period. Surviving larvae exposed to 5 μg of mutant E129A/ml gained 64 ± 8 mg, and those exposed to 50 μg of mutants F130D and V189D gained 17 ± 5 and 12 ± 2 mg, respectively. In contrast, at this higher dose, larvae exposed to L186D gained 116 ± 10 mg, a value comparable to that measured in the absence of toxin.

Membrane Potential Assay

Wild-type Cry9Ca and its R164A mutant have recently been studied, under a variety of experimental conditions, using an osmotic swelling assay (Brunet et al. 2010a) and membrane potential measurements (Brunet et al. 2010b). Both toxins were most effective when tested at pH 10.5, with the electrophysiological assay, in the presence of either 10% (v/v) midgut juice or a cocktail of protease inhibitors. For this reason and because the midgut content of actively feeding lepidopteran insect larvae is highly alkaline (Dow 1984, 1992), these conditions were chosen to evaluate the pore-forming ability of the double mutants described in the present study. In this assay, the electrical potential difference was monitored across the luminal membrane of the epithelial cells of freshly isolated midguts (Peyronnet et al. 1997). After 5 min, during which the midguts were perfused with bathing solution, the tissue was exposed to toxin and either midgut juice (Fig. 3) or protease inhibitors (Fig. 4) for another 5 min, during which perfusion was stopped. During this period, membrane potential decreased somewhat; but in the absence of toxin, it rapidly rose to a value approaching that measured at the beginning of the experiment, as soon as the perfusion was

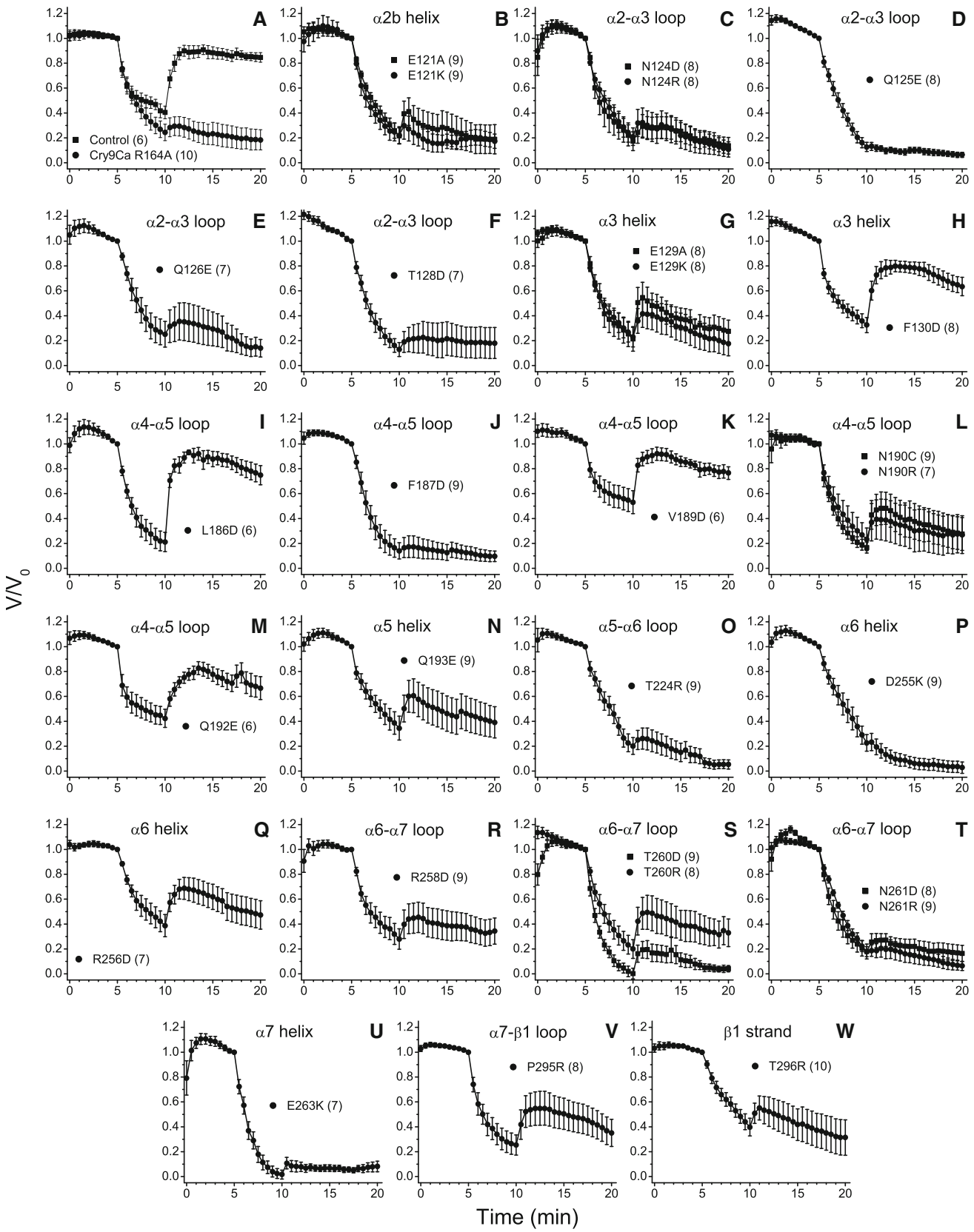
A
Control (6)
Cry9Ca R164A (10)
α2b helix
B
E121A (9)
E121K (9)
α2-α3 loop
C
N124D (8)
N124R (8)
α2-α3 loop
D
Q125E (8)
α2-α3 loop
E
Q126E (7)
α2-α3 loop
F
T128D (7)
α3 helix
G
E129A (8)
E129K (8)
α3 helix
H
F130D (8)
α4-α5 loop
I
L186D (6)
α4-α5 loop
J
F187D (9)
α4-α5 loop
K
V189D (6)
α4-α5 loop
L
N190C (9)
N190R (7)
α4-α5 loop
M
Q192E (6)
α5 helix
N
Q193E (9)
α5-α6 loop
O
T224R (9)
α6 helix
P
D255K (9)
α6 helix
Q
R256D (7)
α6-α7 loop
R
R258D (9)
α6-α7 loop
S
T260D (9)
T260R (8)
α6-α7 loop
T
N261D (8)
N261R (9)
α7 helix
U
E263K (7)
α7-β1 loop
V
P295R (8)
β1 strand
W
T296R (10)
V/V0
Time (min)

◀ **Fig. 3** Effect of domain I interhelical loop mutants on the membrane potential of midgut epithelial cells from *M. sexta* in the presence of midgut juice. Freshly isolated midguts from third-instar larvae were perfused for 5 min with the 122 K solution. The perfusion was stopped, and 1.2 ml of perfusion solution containing 5 μg/ml of the indicated mutant and 10% midgut juice was added directly to the bath. After 5 min, midguts were rinsed with the 122 K solution by resuming the perfusion. V is the membrane potential measured at the indicated times, and V_0 is the membrane potential measured immediately preceding the addition of toxin. For these experiments, V_0 was (−57.2 ± 1.8) mV. Values are means ± SEM (standard error of the mean) for the number of experiments indicated between parentheses

resumed (Figs. 3a, 4a). However, membrane potential remained low in the presence of an active toxin such as the R164A mutant (Figs. 3a, 4a).

In agreement with the toxicity data, most mutants depolarized the midgut epithelial cell membrane efficiently, in the presence of either midgut juice (Fig. 3) or protease inhibitors (Fig. 4). In addition, the three nonlethal double mutants, F130D (Figs. 3h, 4h), L186D (Figs. 3i, 4i) and V189D (Figs. 3k, 4k), were, at best, very poorly active under both experimental conditions. However, mutant Q192E, which was only marginally less toxic than the parental toxin (Table 1), was rather poorly active in the electrophysiological experiments under both sets of conditions (Figs. 3m, 4m). Despite its lower toxicity (Table 1), mutant E129A (Figs. 3g, 4g) was only slightly less active than its parental toxin (Figs. 3a, 4a) and displayed a depolarization rate that was comparable to those measured for mutants E129K (Figs. 3g, 4g), Q193E (Figs. 3n, 4n), T260D (Figs. 3s, 4s), P295R (Figs. 3v, 4v), and P296R (Figs. 3w, 4w) under both experimental conditions. On the other hand, mutants R256D (Fig. 3q) and R258D (Fig. 3r) were slightly less active than their parental toxin in the presence of midgut juice but equally active in the presence of protease inhibitors (Fig. 4q, r). In contrast, mutant N190C was slightly less active than its parental toxin in the presence of protease inhibitors (Fig. 4l) but equally active in the presence of midgut juice (Fig. 3l).

Discussion

The main objective of the present study was to evaluate the influence of charged residues, within surface-exposed loops of domain I, on the pore-forming activity of Cry9Ca. Most mutated residues were located in or very near the α2–α3, α4–α5 and α6–α7 loops because these lie on the same side of the toxin molecule as the domain II loops (Fig. 1a), which are thought to participate directly in the binding of *B. thuringiensis* toxins to their receptors (Gómez et al. 2007; Pigott and Ellar 2007). Moreover, because the pore-forming activity of Cry9Ca was recently found to be particularly sensitive to the environmental pH (Brunet et al. 2010a), electrostatic interactions with its target membrane could be expected to contribute significantly to its mechanism of action.

Most mutations analyzed in the present study, however, had rather little effect on the activity of the toxin, as evaluated from bioassays performed with insect larvae (Table 1) or from their ability to depolarize the apical membrane of epithelial cells in freshly isolated larval midguts (Figs. 3, 4). Most domain I interhelical loop mutants in Cry1Aa that were studied earlier also retained a good pore-forming ability (Lebel et al. 2009). However, many of these latter mutants, in which selected amino acid residues were replaced individually by a cysteine, had a reduced rate of pore formation at pH 10.5, at which the thiol group of this residue is largely ionized. It should nevertheless be pointed out that these experiments were carried out using an osmotic swelling assay protocol in which the brush border membrane vesicles are only exposed to the toxins in solutions of relatively low ionic strength (up to 75 mM KCl depending on the experiments). In contrast, the experiments described in the present communication were performed in a 122 K solution, in which the ionic strength was sufficiently high to greatly attenuate the inhibitory effect of increasing pH to 10.5 on the activity of Cry1Ca (Fortier et al. 2005). As pointed out above, the conditions used in the present study were chosen because of the much poorer activity of Cry9Ca and its single-site mutant R164A in osmotic swelling experiments performed at pH 10.5. Similarly, about half of the mutants described herein were tested in osmotic swelling experiments. Most of them, like their parental toxin R164A (Brunet et al. 2010a), permeabilized the vesicles efficiently at pH 7.5 but displayed at most very modest activity at pH 10.5 (data not shown). These considerations could therefore suggest, in agreement with our earlier conclusion (Fortier et al. 2005), that the influence of electrostatic interactions between the toxin and membrane surface in the process of pore formation diminishes as the ionic strength of the solutions is increased.

Some of the mutations analyzed in the present study did nevertheless affect greatly the activity of Cry9Ca. In particular, mutant F130D, altered near the N-terminal end of its α3-helix, and mutants L186D and V189D, altered within their α4–α5 loops, were almost completely inactive both in vivo and in vitro. The F91S mutation, slightly more conservative than F130D but introduced at the equivalent location in Cry1Ac, also led to reduced toxicity (10- to 100-fold) (Wu and Aronson 1992). Thus, the presence of phenylalanine, or of another aromatic residue at this position, appears to be important for the function of both toxins. As for mutants L186D and V189D, the side chains of both mutated residues extend toward the α3-helix.

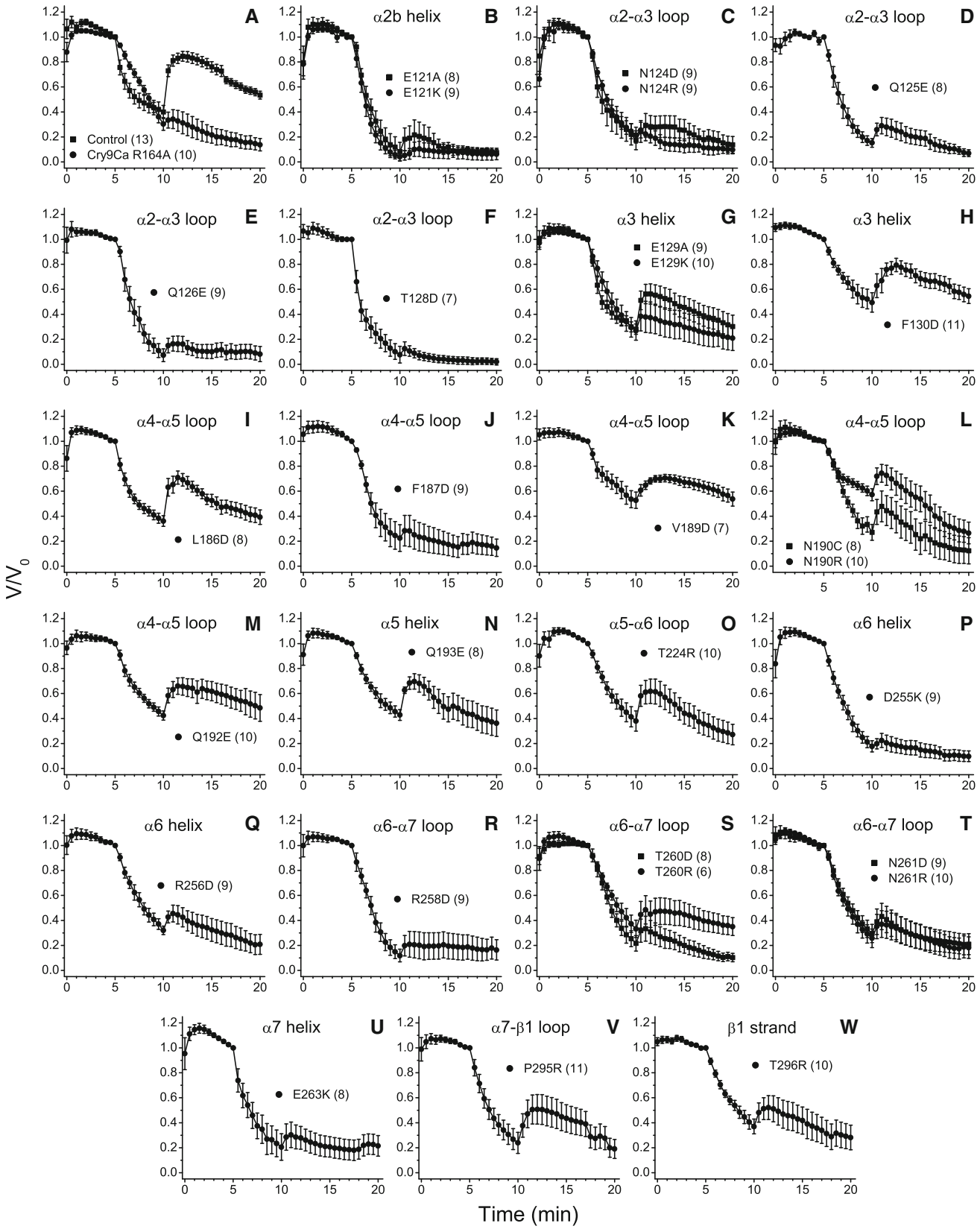

Fig. 4 Effect of domain I interhelical loop mutants on the membrane potential of midgut epithelial cells from *M. sexta* in the presence of protease inhibitors. Experiments were carried out as described in the legend of Fig. 3 except that midgut juice was replaced by a cocktail of protease inhibitors. The composition of this cocktail is given under Materials and Methods. For these experiments, V_0 was (−48.8 ± 1.7) mV

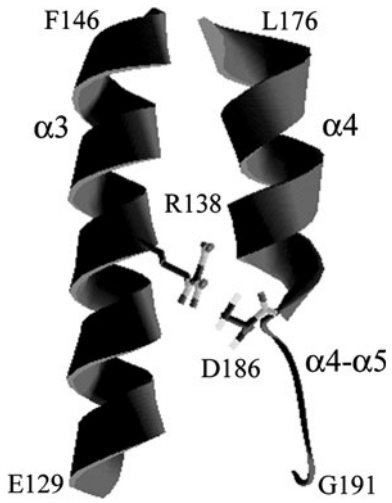

Fig. 5 Possible salt bridge within domain I of the L186D mutant. The orientation of R138 and D186 could allow the formation of a salt bridge, which could prevent a conformational change in which helices α3 and α4 move away from each other, thus contributing to the inactivity of L186D. Only segments of α3, extending from residues 129–146; α4, from residues 176–185; and the α4–α5 loop, from residues 186–191, are displayed

The inactivity of these mutants could result from the formation of a salt bridge between the introduced negative charge and the positive charge of one of the arginine residues of this latter helix (R132 and R138). The possibility of a salt bridge between R138 and D186 is especially well supported by our three-dimensional model of Cry9Ca, which predicts that these two residues may be oriented correctly for such an interaction to occur (Fig. 5). Such a link between the α3-helix and the α4–α5 loop could prevent the hairpin formed by helices α4 and α5 to insert into the membrane as predicted, for example, by the umbrella model (Schwartz et al. 1997; Gazit et al. 1998; Gerber and Shai 2000; Aronson and Shai 2001). The formation of a similar salt bridge appears less likely in the case of the V189D mutant, however, since our model predicts that the side chains of R132 and D189 could not face each other unless the α4–α5 loop was rotated relative to helix α3 by approximately 90° (data not shown). In Cry1Aa, mutant V150C, altered at a location which is equivalent to V189 in Cry9Ca, was not active (Lebel et al. 2009). In contrast, however, the toxicity of a Cry1Ac mutant altered at this same position, V150D, was comparable to that of its wild-type toxin (Kumar and Aronson 1999).

On the other hand, mutant F187D (α4–α5 loop) was quite active both in vivo (Table 1) and in vitro (Figs. 3j, 4j), as was the Cry1Ac F148I mutant, altered at the equivalent position (Kumar and Aronson 1999). While the Cry9Ca mutant N190C, also altered within the α4–α5 loop, retained a pore-forming activity that was comparable to that of its parental toxin, the Cry1Aa mutant Q151C, altered at the equivalent position, formed pores more slowly than wild-type Cry1Aa (Lebel et al. 2009). Although toxic to the larvae (Table 1), the Cry9Ca mutant Q192E, altered within the same loop, was rather poorly active in vitro (Figs. 3m, 4m). Mutants of Cry1Aa and Cry1Ab with substitutions at the equivalent position have also been reported to have a reduced activity. Thus, mutant Y153C from Cry1Aa had a reduced rate of pore formation (Lebel et al. 2009) and mutants Y153A, Y153D and Y153R from Cry1Ab were less toxic than the wild-type toxin and had a reduced ability to inhibit short circuit currents (Chen et al. 1995). Interestingly, while this position is occupied by a glutamine residue (Q192) in Cry9Ca, many other toxins bear a tyrosine residue at the equivalent position. Moreover, on the basis of the functional properties of mutants Y153C from Cry1Aa (Girard et al. 2009) and Cry1Ab (Nuñez-Valdez et al. 2001), Y202A, Y202C and Y202F from Cry4Aa (Pornwiroon et al. 2004) and Y170D, Y170R and Y170L from Cry4Ba (Kanintronkul et al. 2003), it has been concluded that the presence of an aromatic residue at this location is important, or even necessary, for the functioning of these toxins.

Overall, the results of the present study show a remarkably good agreement, with only a few minor exceptions, between the toxicity of the studied mutants and their ability to depolarize the plasma membrane of midgut epithelial cells in the presence of either midgut juice or a cocktail of protease inhibitors. Because Cry9Ca and its R164A mutant display only a rather modest activity at pH 10.5 in the absence of these additions (Brunet et al. 2010b), this correlation lends further support to our hypothesis that the functional properties of Cry9Ca, and probably other *B. thuringiensis* toxins, are strongly influenced by the combined effects of proteases and protease inhibitors present in larval insect midgut juice (Brunet et al. 2010b).

Acknowledgements This work was supported by grants from the Natural Sciences and Engineering Research Council of Canada, the Fonds québécois de la recherche sur la nature et les technologies (FQRNT) and Valorisation-Recherche Québec. J.-F. B. received a graduate student scholarship from the FQRNT.

References

Alcantara EP, Alzate O, Lee MK, Curtiss A, Dean DH (2001) Role of α-helix seven of *Bacillus thuringiensis* Cry1Ab δ-endotoxin in membrane insertion, structural stability, and ion channel activity. Biochemistry 40:2540–2547

Angsuthanasombat C, Uawithya P, Leetachewa S, Pornwiroon W, Ounjai P, Kerdcharoen T, Katzenmeier G, Panyim S (2004) *Bacillus thuringiensis* Cry4A and Cry4B mosquito-larvicidal proteins: homology-based 3D model and implications for toxin activity. J Biochem Mol Biol 37:304–313

Aronson AI, Shai Y (2001) Why *Bacillus thuringiensis* insecticidal toxins are so effective: unique features of their mode of action. FEMS Microbiol Lett 195:1–8

Boonserm P, Davis P, Ellar DJ, Li J (2005) Crystal structure of the mosquito-larvicidal toxin Cry4Ba and its biological implications. J Mol Biol 348:363–382

Boonserm P, Mo M, Angsuthanasombat C, Lescar J (2006) Structure of the functional form of the mosquito larvicidal Cry4Aa toxin from *Bacillus thuringiensis* at a 2.8-angstrom resolution. J Bacteriol 188:3391–3401

Bravo A, Gill SS, Soberón M (2007) Mode of action of *Bacillus thuringiensis* Cry and Cyt toxins and their potential for insect control. Toxicon 49:423–435

Brunet J-F, Vachon V, Juteau M, Van Rie J, Larouche G, Vincent C, Schwartz J-L, Laprade R (2010a) Pore-forming properties of the *Bacillus thuringiensis* toxin Cry9Ca in *Manduca sexta* brush border membrane vesicles. Biochim Biophys Acta 1798:1111–1118

Brunet J-F, Vachon V, Marsolais M, Van Rie J, Schwartz J-L, Laprade R (2010b) Midgut juice components affect pore formation by the *Bacillus thuringiensis* insecticidal toxin Cry9Ca. J Invertebr Pathol 104:203–208

Chen XJ, Curtiss A, Alcantara E, Dean DH (1995) Mutations in domain I of *Bacillus thuringiensis* δ-endotoxin Cry1Ab reduce the irreversible binding of toxin to *Manduca sexta* brush border membrane vesicles. J Biol Chem 270:6412–6419

Coux F, Vachon V, Rang C, Moozar K, Masson L, Royer M, Bes M, Rivest S, Brousseau R, Schwartz J-L, Laprade R, Frutos R (2001) Role of interdomain salt bridges in the pore-forming ability of the *Bacillus thuringiensis* toxins of Cry1Aa and Cry1Ac. J Biol Chem 276:35546–35551

de Maagd RA, Bravo A, Berry C, Crickmore N, Schnepf HE (2003) Structure, diversity, and evolution of protein toxins from spore-forming entomopathogenic bacteria. Annu Rev Genet 37: 409–433

Dow JAT (1984) Extremely high pH in biological systems: a model for carbonate transport. Am J Physiol Regul Integr Comp Physiol 246:R633–R635

Dow JAT (1992) pH gradients in lepidopteran midgut. J Exp Biol 172:355–375

Fernández LE, Pérez C, Segovia L, Rodríguez MH, Gill SS, Bravo A, Soberón M (2005) Cry11Aa toxin from *Bacillus thuringiensis* binds its receptor in *Aedes aegypti* mosquito larvae through loop α-8 of domain II. FEBS Lett 579:3508–3514

Fortier M, Vachon V, Kirouac M, Schwartz J-L, Laprade R (2005) Differential effects of ionic strength, divalent cations and pH on the pore-forming activity of *Bacillus thuringiensis* insecticidal toxins. J Membr Biol 208:77–87

Fortier M, Vachon V, Frutos R, Schwartz J-L, Laprade R (2007) Effect of insect larval midgut proteases on the activity of *Bacillus thuringiensis* Cry toxins. Appl Environ Microbiol 73: 6208–6213

Galitsky N, Cody V, Wojtczak A, Ghosh D, Luft JR, Pangborn W, English L (2001) Structure of the insecticidal bacterial δ-endotoxin Cry3Bb1 of *Bacillus thuringiensis*. Acta Crystallogr D Biol Crystallogr 57:1101–1109

Gazit E, La Rocca P, Sansom MSP, Shai Y (1998) The structure and organization within the membrane of the helices composing the pore-forming domain of *Bacillus thuringiensis* δ-endotoxin are consistent with an "umbrella-like" structure of the pore. Proc Natl Acad Sci USA 95:12289–12294

Gerber D, Shai Y (2000) Insertion and organization within membranes of the δ-endotoxin pore-forming domain, helix 4-loop–helix 5, and inhibition of its activity by a mutant helix 4 peptide. J Biol Chem 275:23602–23607

Girard F, Vachon V, Lebel G, Préfontaine G, Schwartz J-L, Masson L, Laprade R (2009) Chemical modification of *Bacillus thuringiensis* Cry1Aa toxin single-cysteine mutants reveals the importance of domain I structural elements in the mechanism of pore formation. Biochim Biophys Acta 1788:575–580

Gómez I, Pardo-López L, Muños-Garay C, Fernandez LE, Pérez C, Sánchez J, Soberón M, Bravo A (2007) Role of receptor interaction in the mode of action of insecticidal Cry and Cyt toxins produced by *Bacillus thuringiensis*. Peptides 28:169–173

Griffitts JS, Aroian RV (2005) Many roads to resistance: how invertebrates adapt to Bt toxins. Bioessays 27:614–624

Grochulski P, Masson L, Borisova S, Pusztai-Carey M, Schwartz J-L, Brousseau R, Cygler M (1995) *Bacillus thuringiensis* CryIA(a) insecticidal toxin: crystal structure and channel formation. J Mol Biol 254:447–464

Guex N, Peitsch MC (1997) SWISS-MODEL and the Swiss-PdbViewer: an environment for comparative protein modelling. Electrophoresis 18:2714–2723

Guo S, Ye S, Liu Y, Wei L, Xue J, Wu H, Song F, Zhang J, Wu X, Huang D, Rao Z (2009) Crystal structure of *Bacillus thuringiensis* Cry8Ea1: an insecticidal toxin toxic to underground pests, the larvae of *Holotrichia parallela*. J Struct Biol 168:259–266

Gutierrez P, Alzate O, Orduz S (2001) A theoretical model of the tridimensional structure of *Bacillus thuringiensis* subsp. *medellin* Cry11Bb toxin deduced by homology modelling. Mem Inst Oswaldo Cruz 96:357–364

Ho SN, Hunt HD, Horton RM, Pullen JK, Pease RL (1989) Site-directed mutagenesis by overlap extension using the polymerase chain reaction. Gene 77:51–59

Kanintronkul Y, Sramala I, Katzenmeir G, Panyim S, Angsuthanasombat C (2003) Specific mutations within the α4–α5 loop of the *Bacillus thuringiensis* Cry4B toxin reveal a crucial role for Asn-166 and Tyr-170. Mol Biotechnol 24:11–19

Kumar ASM, Aronson AI (1999) Analysis of mutations in the pore-forming region essential for insecticidal activity of a *Bacillus thuringiensis* δ-endotoxin. J Bacteriol 181:6103–6107

Lambert B, Buysse L, Decock C, Jansens S, Piens C, Saey B, Seurinck J, Van Audenhove K, Van Rie J, Van Vliet A, Peferoen M (1996) A *Bacillus thuringiensis* insecticidal crystal protein with a high activity against members of the family Noctuidae. Appl Environ Microbiol 62:80–86

Lebel G, Vachon V, Préfontaine G, Girard F, Masson L, Juteau M, Bah A, Larouche G, Vincent C, Laprade R, Schwartz J-L (2009) Mutations in domain I interhelical loops affect the rate of pore formation by the *Bacillus thuringiensis* Cry1Aa toxin in insect midgut brush border membrane vesicles. Appl Environ Microbiol 75:3842–3850

Li J, Carroll J, Ellar DJ (1991) Crystal structure of insecticidal δ-endotoxin from *Bacillus thuringiensis* at 2.5 Å resolution. Nature 353:815–821

Li J, Derbyshire DJ, Promdonkoy B, Ellar DJ (2001) Structural implications for the transformation of the *Bacillus thuringiensis* δ-endotoxins from water-soluble to membrane-inserted forms. Biochem Soc Trans 29:571–577

Likitvivatanavong S, Aimanova KG, Gill SS (2009) Loop residues of the receptor binding domain of *Bacillus thuringiensis* Cry11Ba toxin are important for mosquitocidal activity. FEBS Lett 583: 2021–2030

Lin Y, Fang G, Cai F (2008) The insecticidal crystal protein Cry2Ab10 from *Bacillus thuringiensis*: cloning, expression, and structure simulation. Biotechnol Lett 30:513–519

Masson L, Préfontaine G, Péloquin L, Lau PCK, Brousseau R (1990) Comparative analysis of the individual protoxin components in P1 crystals of *Bacillus thuringiensis* subsp. *kurstaki* isolates NRD-12 and HD-1. Biochem J 269:507–512

Masson L, Mazza A, Gringorten L, Baines D, Aneliunas V, Brousseau R (1994) Specificity domain localization of *Bacillus thuringiensis* insecticidal toxins is highly dependent on the bioassay system. Mol Microbiol 14:851–860

Morse RJ, Yamamoto T, Stroud RM (2001) Structure of Cry2Aa suggests an unexpected binding epitope. Structure 9:409–417

Nuñez-Valdez M-E, Sánchez J, Lina L, Güereca L, Bravo A (2001) Structural and functional studies of α-helix 5 region from *Bacillus thuringiensis* Cry1Ab δ-endotoxin. Biochim Biophys Acta 1546:122–131

Ohba M, Mizuki E, Uemori A (2009) Parasporin, a new anticancer protein group from *Bacillus thuringiensis*. Anticancer Res 29: 427–434

Peitsch MC (1995) Protein modeling by e-mail. Bio/Technol 13: 658–660

Peitsch MC (1996) ProMod and Swiss-Model: internet-based tools for automated comparative protein modelling. Biochem Soc Trans 24:274–279

Peyronnet O, Vachon V, Brousseau R, Baines D, Schwartz J-L, Laprade R (1997) Effect of *Bacillus thuringiensis* toxins on the membrane potential of lepidopteran insect midgut cells. Appl Environ Microbiol 63:1679–1684

Pigott CR, Ellar DJ (2007) Role of receptors in *Bacillus thuringiensis* crystal toxin activity. Microbiol Mol Biol Rev 71:255–281

Pornwiroon W, Katzenmeier G, Panyim S, Angsuthanasombat C (2004) Aromaticity of Tyr-202 in the α4–α5 loop is essential for toxicity of the *Bacillus thuringiensis* Cry4A toxin. J Biochem Mol Biol 37:292–297

Schnepf E, Crickmore N, Van Rie J, Lereclus D, Baum J, Feitelson J, Zeigler DR, Dean DH (1998) *Bacillus thuringiensis* and its pesticidal crystal proteins. Microbiol Mol Biol Rev 62:775–806

Schwartz J-L, Juteau M, Grochulski P, Cygler M, Préfontaine G, Brousseau R, Masson L (1997) Restriction of intramolecular movements within the Cry1Aa toxin molecule of *Bacillus thuringiensis* through disulfide bond engineering. FEBS Lett 410:397–402

Wei J-Z, Hale K, Carta L, Platzer E, Wong C, Fang S-C, Aroian RV (2003) *Bacillus thuringiensis* crystal proteins that target nematodes. Proc Natl Acad Sci USA 100:2760–2765

Wu D, Aronson AI (1992) Localized mutagenesis defines regions of the *Bacillus thuringiensis* δ-endotoxin involved in toxicity and specificity. J Biol Chem 267:2311–2317

Xia L-Q, Zhao X-M, Ding X-Z, Wang F-X, Sun Y-J (2008) The theoretical 3D structure of *Bacillus thuringiensis* Cry5Ba. J Mol Model 14:843–848

Yamaguchi T, Sahara K, Bando H, Asano S (2008) Discovery of a novel *Bacillus thuringiensis* Cry8D protein and the unique toxicity of the Cry8D-class proteins against scarab beetles. J Invertebr Pathol 99:257–262

Zhao X-M, Xia L-Q, Ding X-Z, Wang F-X (2009) The theoretical three-dimensional structure of *Bacillus thuringiensis* Cry5Aa and its biological implications. Protein J 28:104–110